High-power LED array design and assembly for practical photodynamic therapy research

Eric M Kercher,[a,b] Kai Zhang,[a,b] Matt Waguespack,[a,b] Ryan T Lang,[a,b] Alejandro Olmos,[c] Bryan Q Spring[a,b,d,*]

[a]Translational Biophotonics Cluster, Northeastern University, Boston, MA, USA, 02115
[b]Department of Physics, Northeastern University, Boston, MA, USA, 02115
[c]Department of Health Sciences, Northeastern University, Boston, MA, USA, 02115
[d]Department of Bioengineering, Northeastern University, Boston, MA, USA, 02115

Structured Abstract

Significance. Commercial lasers, lamps, and LED light sources have stimulated the clinical translation of photodynamic therapy (PDT). Yet, the continued exploration of new photosensitizers (PSs) for PDT often requires separate activation wavelengths for each agent being investigated. Customized light sources for such research frequently come at significant financial or technical cost, especially when compounded over many agents and wavelengths.

Aim. LEDs offer potential as a cost-effective tool for new PS and multi-PS photodynamic research. A low-cost-per-wavelength tool leveraging high-power LEDs to facilitate efficient and versatile research is needed to further accelerate research in the field.

Approach. Here, we developed and validated a high-power LED array system for benchtop PDT with a modular design for efficient switching between wavelengths that overcomes many challenges in light source design. We describe assembly of a low-cost, LED module plus the supporting infrastructure, software, and protocols to streamline typical *in vitro* PDT experimentation.

Results. The LED array system is stable at intensities in excess of 100 mW/cm^2 with 2.3% variation across the illumination field, competitive with other custom and commercial devices. To demonstrate efficacy and versatility, a primary ovarian cancer cell line was treated with two widely used PSs, aminolevulinic acid and verteporfin, using the LED modules at a clinically relevant 50 J/cm^2 light dose that induced over 90% cell death for each treatment.

Conclusions. This work provides the community with a tool for new PS and multi-PS benchtop photodynamic research that, unlike most commercial light sources, affords the user a low barrier to entry and low cost-per-wavelength with the goal of illuminating new insights at the forefront of PDT.

Keywords: LED, PDT, ALA, BPD, verteporfin

***Corresponding Author:** Bryan Q Spring**,** E-mail: b.spring@northeastern.edu Phone: 617-373-5303

1 Introduction

Use of light to treat disease was first discovered by the ancient Egyptians, who discovered that application of certain plants combined with sunlight exposure ("heliotherapy") could treat vitiligo[1]. The advent of modern phototherapy followed naturally from the invention of broadband, ultra-violet (UV) sources like mercury and arc lamps, which were well-suited for scientific investigation. UV light was first used to successfully treat lupus vulgaris and psoriasis in combination with methoxypsoralen[2] (the active ingredient in the same plants used by the Egyptians millennia before). This formed the basis for psoralen-and-UVA (PUVA) therapy and was used to treat many more dermatological indications[3]. Later, narrowband UVB (311–313 nm) replaced broadband UV as an easier and more effective treatment method and is still used today[4,5].

The serendipitous discovery of "photodynamic action" by Raab and Von Tappeiner in 1900 spawned the related field of photodynamic therapy (PDT); the distinction among phototherapies being the direct induction of cytotoxicity by light through a mediating chemical, or photosensitizer (PS)[6]. This effect was largely ignored until Dougherty and colleagues completed the first large-scale study of PDT to treat solid tumors with hematoporphyrin derivative (now approved as Photofrin®) in 1978[7], enabled by the invention of the helium-neon laser (632.8 nm) just 16 years before[8]. Since then, the continued development of new laser sources have accelerated the development of new PSs and applications for clinical PDT[9].

Presently, light sources used for photoactivation can be organized into three categories[10,11]. First and most widely implemented are lasers, which are desirable for their efficient, high-power, and coherent output. Some laser cavity designs used for PDT include argon dye, Cu- and Au-vapor, frequency-doubled Nd:YAG, solid-state, and semiconductor diodes[10,12]. Lasers also generally offer the highest density of photons for fiber coupling and endoscopic or interstitial light delivery. Second, filtered lamps provide relatively uniform wide-field illumination but have not found much use outside of dermatological

settings[10]. Finally, light-emitting diodes (LEDs) disperse incoherent light from a small semiconductor with an intensity proportional to the current across the diode. They offer a compromise between lasers and lamps and can reach intensities above 1 W[13]. LEDs are also versatile when assembled into linear arrays for endoscopic light delivery or 2D arrays which can illuminate broad areas comparable to most lamps[10,11].

In the many reviews and historical accounts of PDT[9,11,14–20], the discussion of light sources takes a lower priority to noteworthy chemical, physical, and biological discoveries and insights regarding PS development and clinical efficacy (with some exceptions[10,11]). Despite the frequent lack of emphasis, light delivery itself is widely appreciated as a fundamental component of photodynamic research. Developing PDT for a specific disease requires the right combination of PS, light source, and light dose, and it depends largely on the disease morphology; a unique light source is often required to study each new PS under different applications[17].

To illustrate this, three FDA approved agents serve as informative examples. Interestingly, all three are approved using different light sources for photoactivation. First, aminolevulinic acid (ALA, Levulan®), approved in 1999 for treatment of mild to moderate actinic keratosis (AK), is activated using a blue fluorescent lamp (BLU-U® Blue Light Photodynamic Therapy Illuminator) at 417 ± 5 nm wavelength with a recommended dose of 10 J/cm^2 over 16 minutes and 40 seconds[21]. Second, methyl aminolevulinate (MAL, Metvixia®) was FDA approved for AK in 2004 paired with a metal halogen lamp at 570–670 nm (CureLight Broadband, Model CureLight 01). Based on prior pre-clinical data[22], a follow-up clinical trial in 2008 (NCT00304239) demonstrated LED illumination at 630 ± 5 nm (Aktilite® CL128) to be a more effective source for MAL activation. In so doing, the recommended light dose was decreased from 75 J/cm^2 over 8–12 minutes using the broadband source to 37 J/cm^2 over 7–10 minutes using the LED array, consistent with others' findings[23,24]. Although effective, treatment of AKs and non-melanoma

77 skin cancers with topical ALA/MAL requires a relatively long treatment time and causes a moderate to
78 severe burning sensation in many patients[25].

79 Third, benzoporphyrin derivative (BPD or verteporfin, Visudyne®), approved in 2000 to treat the
80 wet form of age-related macular degeneration (AMD), is activated via laser at 689 ± 3 nm. The
81 recommended dosing strategy is 50 J/cm^2 at 600 mW/cm^2 over 1 minute and 23 seconds[26], in stark contrast
82 with lower intensity AK treatment guidelines. The difference in light source and dosing strategies between
83 ALA/MAL and verteporfin are simply explained by the physical differences in disease presentation.
84 Despite other side effects, verteporfin PDT in the eye avoids sensory nerves responsible for pain, allowing
85 for a much higher light intensity. In addition, the size of the treatment area (abnormal choroidal
86 neovasculature that grows into the macula) is much smaller than typical AK lesions. These and other
87 factors make a laser source ideal for treatment of AMD, whereas an LED array is more suited for large
88 and/or disperse dermatological indications.

89 Lasers, despite the advantages mentioned, present a formidable cost per wavelength and require
90 special safety equipment and protocols during use. Additionally, in cases where a direct comparison is
91 possible, researchers have found LEDs and lasers do not differ in their treatment efficacy[23,27–30], while
92 others have shown LEDs are just as effective as lamps[22,29] and more effective than sunlight[31]. Furthermore,
93 LEDs are now widely used to treat many dermatological diseases[12,32], and a growing body of work
94 suggests LEDs will have a significant role to play in the future of PDT.

95 Excitement around the use of LEDs for PDT, however, has been stymied by financial and technical
96 hurdles. Existing LED-PDT sources remain expensive and caution should be taken when employing these
97 devices[33]. Furthermore, reports of clever adaptations of non-clinical LED sources for PDT including
98 dental curing lights[13,34], traffic lamps[35], and lighting fixtures[29,36] suggest a lack of variety, versatility, or
99 accessibility in available commercial LED sources. This may be explained, at least in part, by a lack of

competition and limited market size that has discouraged an exciting and robust industry. Those with more specific irradiation requirements, and the appropriate motivation and funding, have reported custom-assembled LED sources for various applications[30,37–41], albeit with limited output powers that require tedious experimental protocols. A light source or system that is cost-effective and generalizable to multiple PSs has not yet been reported.

Here we introduce a protocol for custom LED array assembly and supporting infrastructure for cost-effective and versatile PDT research that considers and overcomes many challenges in LED array design. The device is capable of output powers in excess of 100 mW/cm^2, competitive with most commercial LED and laser sources, and a modular design enables easy switching of wavelengths for research with different PSs. The infrastructure surrounding the module is designed to streamline the experimentation process and allows the user to monitor the LED temperature in real time using a custom software interface and data acquisition card. The viability of these features is demonstrated via treatment of monolayer cell cultures using both ALA- and BPD-PDT. This work improves on a growing trend of LED-PDT research and will aid current and future laboratories in their photodynamic research, especially with the emergence of next-generation photosensitizers.

2 Materials and Methods

2.1 LED Module Design and Assembly

The LED module is designed around an aluminum-substrate printed circuit board (PCB) to maximize heat flow away from the LEDs. This design choice constrains the selection of electronics to only surface-mounted components. Circuits were designed to connect four rows of four 690 nm LEDs (1W Infrared LED, Shenzen Fedy Technology Co.) or six 635 nm LEDs (PLR3535AA000, Plessy Semiconductors) in parallel with 45 W, 10 Ω current limiting resistors (TKH45P10R0FE-TR, Ohmite). A thermistor

(B57452V5103J062, Epcos (TDK)) and a 499 Ω resistor (RNCP0805FTD499R, Stackpole Electronics Inc.) circuit were also included, with the thermistor placed in the center of the LED array to enable real-time measurements of the board temperature. The full circuit required an 8-pin connector that was made from a Dupont connector kit (WYTP07-KIT, WayinTop). The complete circuit board was designed using electronic AutoCAD software (Eagle, Autodesk) and manufactured by a PCB fabrication service (PCB Cart).

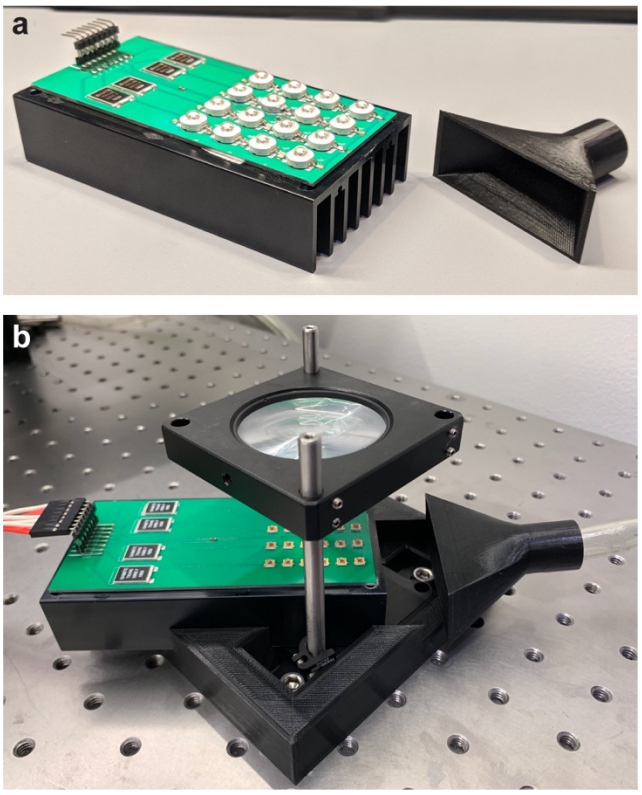

Fig. 1 Custom designed, high power, modular LED array for PDT. (**a**) 690 nm LED module aside a 3D-printed nozzle for air cooling. (**b**) 635 nm LED module mounted on a 3D-printed brace with focusing optic above. A plexiglass surface with an aperture (not shown) is secured directly above the lens on which a well plate is placed for PDT experimentation.

To assemble the board, the components were applied to the PCB via solder paste (EP256, Kester) and, after all the components were added, a hot air gun (898D Soldering Station, Vivohome) set to 400°C was used to solder each component in place. To do this, the PCB was supported with a third hand (01902, Neiko) and the hot air gun was directed at the PCB from 3–4 cm below. A digital multimeter (DMM, WH5000A, AstroAI) was used to confirm that successful connections were achieved. The PCB was then mated to a heat sink (M-B012, Cincon) with a thin layer of thermal paste (Protronix-PST-D Series 7, Protronix), and 6 drops of super glue (PR40, 3M), three on each side, were added along the sides of the PCB to secure it in place (Fig. **1**).

2.2 Supporting Electronics and Optomechanics

The LED circuit was connected to a 30V/5A power supply (HY3005F-3, Dr.meter) with an intermediate single channel 5 V relay (MK1LU5V6P, Ficbox) to enable programmable LED modulation via a USB

data acquisition card (DAQ, USB-6001, National Instruments). The relay was wired to the 5 V power supply, digital ground, and digital I/O channel on the DAQ. The thermistor circuit was also wired to the 5 V DAQ power, with differential signal measured between analog input and ground channels. A subminiature version A (SMA) coaxial connector (8541674577, Maxmoral) was augmented with signal and ground wires in order to read the analog power meter signal through the DAQ from the SMA output on the power meter. The DAQ was connected to a laptop placed next to the experimental setup via USB to USB-c cable (National Instruments). A complete wiring diagram is provided in Fig. **S1**.

The LED module was placed on the surface of an optics table via a custom 3D-printed brace (Ender 5, Comgrow) (Fig. **1b**, Fig. **S2a**) that secures the module to a vertical cage mounting system (CPVM, Thorlabs).. Alternatively, an aluminum breadboard (MB12, Thorlabs) may be used for a mobile cart design or if an optics table is not available. A diffuser-lens pair was placed above the LED module using a 2-inch cage mount (LCP01, Thorlabs) to focus and smooth the light field. The choice of the focusing lens was determined empirically between a Fresnel lens (FRP232, Thorlabs) and an aspheric condenser lens (ACL5040U-DG6-A, Thorlabs), with a 600-grit diffuser (DG20-600, Thorlabs) mounted just below each optic. A power meter sensor (S130C, Thorlabs), connected to a compatible power meter (PM100D, Thorlabs), was placed above, but off-center to, the mounted optic. The lens was then adjusted along the z-axis to maximize the power transmission and determine the height of maximum collimation (*i.e.*, the focal point of the lens). Both lenses allowed similar power transmission, but the Fresnel lens was found to produce a more uniform light field with a larger spot size than the condenser lens and was therefore chosen for the ensuing experiments.

A platform on which to place a well plate for typical *in vitro* PDT experimentation was fashioned from a transparent plexiglass board (SL-AS6, 12×12×1/4-inch, SimbaLux). The board was covered in light-blocking tape (T205-1.0, Thorlabs), except for a 3.85×3.85-cm opening in the center. Two 3/8-inch

holes were drilled on the side of the board and secured to two 4-inch optical posts (TR4, Thorlabs) mounted (UPH1, Thorlabs) to the optics table using 5/8-inch screws (SH25S063, Thorlabs). This fixed the plate height at 4 inches above the table and x-y adjustments were made to align the aperture above the lens.

Since cooling of the module is paramount, we used a compressed air line to provide active cooling of the LED module. A fan could be used in place of the compressed air. Approximately 1 meter of 3/8-inch tubing was connected to the air outlet valve on one end and to a 3D-printed nozzle (Fig. **1**, Fig. **S2b**) on the other. The nozzle was designed to match the cross-section of the heat sink and provide uniform airflow through the fins. It was secured to the table via two 2-inch optics posts (TR2, Thorlabs) combined with a right-angle clamp (RA90, Thorlabs) and a fixed position lens mount (NRC MH-2P, Newport) such that the air was directed through the heat sink fins.

2.3 Software

We employed MATLAB's (R2019b, The MathWorks) data acquisition toolbox to interface with the DAQ via custom software application, ExpressPDT, written with MATLAB's application programming software App Designer (Fig. **S3**). Note that compatibility of the data acquisition toolbox restricts full operation of the software (*i.e.*, connection to the DAQ and relay control) to Windows operating systems. However, ExpressPDT may still be used as a PDT planning tool on any operating system.

2.4 Thermistor Model and Calibration

A thermistor is a resistor whose resistance changes predictably with temperature. We employed this device in a simple voltage divider circuit to measure the on-board temperature of the LEDs in real-time. For negative temperature coefficient (NTC) thermistors, the resistance R varies exponentially with temperature T according to

$$R = R_0 e^{\beta\left(\frac{1}{T}-\frac{1}{T_0}\right)} \quad (1)$$

where R_0 is a known resistance at some temperature T_0, and β is fundamental property of the thermistor. Grouping the constant terms together and assuming β is constant, eq. (1) can be rewritten to show that,

$$R = R_\infty e^{\frac{\beta}{T}} \quad (2)$$

where R_∞ is the resistance of the thermistor at very high temperatures. This model is easily linearized

$$\ln R = \frac{\beta}{T} + \ln R_\infty \quad (3)$$

and can be fit using the variables *ln R* and *1/T* in order to extract β and ln R_∞ as slope and intercept via linear regression. The final step is to connect the thermistor resistance to the voltage measured by the DAQ. The equation describing a simple voltage dividing circuit is

$$\frac{V}{R} = \frac{V_+}{R + R_s} \quad (4)$$

where V and R are the thermistor voltage and resistance, respectively, V_+ is the supply voltage, and R_s is the resistance of the static resistor. Combining eq. (3) and (4) and rearranging terms gives the temperature (in Celsius) as a function of thermistor voltage:

$$T(V) = \frac{\beta}{\ln\frac{R_s}{R_\infty}\left(\frac{V_+}{V} - 1\right)} - 273.15 \quad (5)$$

Although β (and therefore, R_∞) varies slightly with temperature, the LEDs are constrained to a ~20°C operating range over which β changes by < 1%, so the assumption of constant β is valid for monitoring the LED array board. We also assume a constant 5 V supply voltage V_+ and 499 Ω resistance R_s.

The parameters β and R_∞ were determined experimentally for each LED module by measuring the thermistor voltage across a range of temperatures. First, approximately 0.2 mL of thermal paste was placed on the thermistor and the module was refrigerated at 4°C for 2 hours. The module was then reconnected

to the power supply and a thermocouple connected to the DMM was inserted into the thermal paste to determine the temperature of the thermistor. Using ExpressPDT's calibration mode, the temperature and thermistor signal were recorded simultaneously as the module returned to room temperature. The LEDs were then turned on at low power to facilitate further warming of the module at approximately 1 degree every 5–10 seconds. The LEDs were turned off and recording ceased once the module reached 65°C; 40–50 data points were collected in total for each module. Once the calibration procedure was complete, the thermal paste was cleaned from the LED module using cotton swabs and optic wipes dampened with isopropyl alcohol. Data was linearized and fit to eq. (3) using Prism 8 (GraphPad); best fit values β and R_∞ are reported with their standard errors (SE). These values were programmed into ExpressPDT for automated temperature monitoring using eq. (5).

2.5 Module characterization

The emission spectrum of each LED module was measured with a spectrometer (Amadeus AMA01338, Ocean Optics) at room temperature (21°C), and then again at 38°C to characterize the effect of temperature on the spectral emission. The LED supply voltage was then adjusted so that the power meter read ~100 mW/cm^2 peak power at the plate surface. Once the temperature stabilized, the temperature and power were recorded for 7 minutes at 1 second intervals using ExpressPDT. To assess the power delivered to each well of a cell culture 24-well plate, the module was turned on and allowed to stabilize at 39°C. The power at the plate surface in each quadrant of the aperture was measured 3 times with a power meter to determine the intensity given to each well in 2×2-well experimental group. Average temperature and intensity are reported as mean ± standard deviation (SD) with the coefficient of variation (CV, defined as SD divided by mean) provided where useful.

2.6 Cell Culture and PDT

Human primary high-grade serous ovarian cancer line (Powder, Cellaria Biosciences) was cultured in T75 Flasks (1256685, Thermo Scientific) according to a protocol recommended by Cellaria Biosciences in a humidified incubator at 5% CO_2 and 37°C. Powder cells were cultured in Renaissance Essential Tumor Medium (RETM) and RETM Supplement (CM-0001, Cellaria Biosciences) completed with 6.3% heat-inactivated fetal bovine serum (FBS, SH30071.03HI, Hyclone™ GE Healthcare Life Sciences) and 1% Penicillin/Streptomycin (BP295950, Fisher BioReagents).

Before plating, RETM was prepared by diluting stock media to 3% FBS and was used throughout the experiment. During passaging, cells were lifted with 0.25% Trypsin EDTA (25053CI, Corning), washed in phosphate buffered saline (PBS, 70011069, Gibco), and suspended at 20,000 cells/mL in RETM at 3% serum. One mL of cell solution was added to each well of a black-walled, 24-well plate (P241.5HN, Cellvis) and allowed to grow for 3 days. PS was administered at 0.5 mM ALA (A3785, Sigma Aldrich) or 0.5 μM verteporfin (Visudyne®, QLT Phototherapeutics, Inc.) in media and incubated for 4.5 or 2 hours, respectively. Just before illumination, all wells were aspirated and replaced with fresh media.

In order to increase protocol efficiency, experimental groups were organized into 2×2-well groups (4 biological replicates) to be illuminated simultaneously. Six treatment groups in each 24-well plate included 3 controls: No PS + 0 J/cm^2, No PS + 50 J/cm^2, and PS + 0 J/cm^2, plus 3 treatment groups given PS + 10, 20, and 50 J/cm^2. For ALA-PDT, the average irradiance of the 635 nm module in each quadrant was 86.6 mW/cm^2 at a stable module temperature of 39°C, and the total plate illumination time was 25 minutes. For BPD-PDT, the average irradiance of the 690 nm module in each quadrant was 79.7 mW/cm^2 at 39°C, with a total plate illumination time of 27 minutes and 10 seconds. Laser safety goggles (100-38-245, Laser Safety Industries) with OD2+ at >630 nm were worn during illumination. All work with PSs was done in subdued light and plates were protected from light with aluminum foil except during PDT.

Cell culture viability was assessed with fluorescent live/dead staining 24 hours after light treatment using flow cytometry (FC) and validated with confocal microscopy. Three out of the 4 wells from each group were collected and stained with Live/Dead Fixable Green (L-34970, Life Technologies) for 30 minutes at 4°C protected from light. Cells in suspension were included in this analysis by collecting the supernatant before lifting the cells. After staining, samples were washed a further 2 times in PBS, resuspended in 300 µL PBS, and immediately analyzed using a flow cytometer (Attune NxT, ThermoFisher). After the cells were collected from the plate for FC analysis, the 4th well was washed with PBS (discarding the supernatant) and stained with a 1:60 dilution of Acridine Orange/Propidium Iodide (F23001, Logos Biosystems) in media and immediately imaged using a laser-scanning confocal microscope (LSM 800, Zeiss). Viability is reported as the average ± SE percent cell death relative to the no treatment control.

3 Results

3.1 Thermistor Calibration

The thermistors on each module demonstrated ideal behavior across the range of operating temperatures (20–40°C, Fig. **2**). Temperature and voltage were fit to a linearized model (eq. (3)) with slope β and intercept R_∞ (Fig. **S4**). For the 635 nm array we found $\beta = 4442 \pm 16$ K and $R_\infty = 3.34 \pm 0.17$ mΩ. For the 690 nm array we determined $\beta = 4279 \pm 7$ K and $R_\infty = 5.37 \pm 0.13$ mΩ, in agreement with manufacturer specified values. These data were then

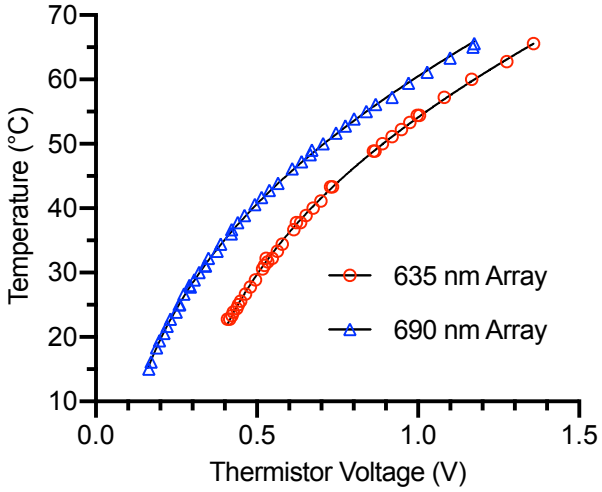

Fig. 2 Thermistor Calibration. Temperature and voltage measurements (symbols) were used to find the best fit values for eq. (5) (lines). For clarity, the 635 nm array data set is shifted horizontally by +0.2 volts.

programmed into ExpressPDT software using eq. (5) to enable real-time module temperature monitoring during treatment.

3.2 LED Module Characterization

At 38°C, the LED emission underwent slight red-shifting and loss of intensity compared to room temperature (Fig. **3**). The 635 nm spectrum red shift was less than the spectrometer resolution (< 2 nm), and the relative intensity was 94% of the room temperature spectrum. The 690 nm LED fidelity was slightly more impacted at 38°C with a red shift of 4 nm at 86% of room temperature power. These shifts were not enough to compromise the PS excitation efficiency.

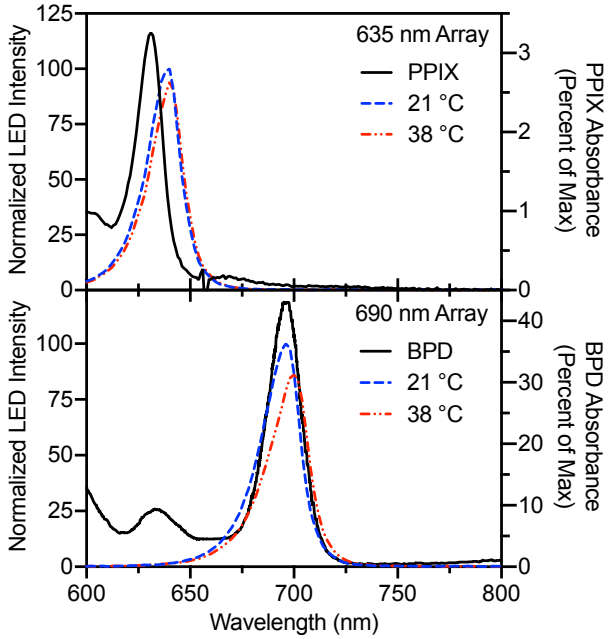

Fig. 3 LED Array spectral emission (left y-axis) at room temperature (21°C) and operating temperature (38°C) align with their respective photosensitizer absorption spectra (right y-axis). Relative intensities are preserved between low and high temperature spectra after normalization.

Thermal stability was assessed over a 7-minute trial by measuring the temperature and peak power of the LED array at 1-second intervals. Both the 635 nm and 690 nm boards displayed less than 1% variation in both variables over that time frame (Fig. **4**). Specifically, the 635 nm array was stable at 36.8 ± 0.2°C (CV = 0.42%) with an output of 104.9 ± 0.1 mW/cm^2 (CV = 0.13%). Similarly, the 690 nm array was stable at 32.1 ± 0.1°C (CV = 0.40%) with an output of 102.9 ± 0.1 mW/cm^2 (CV = 0.13%).

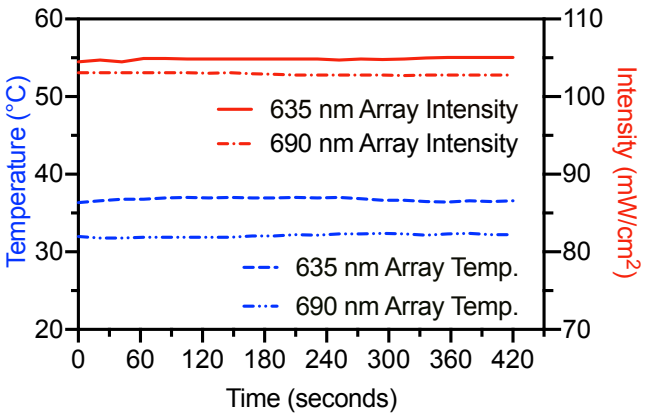

Fig. 4 Both LED modules are stable at operating temperature and demonstrated less than 1% variation in on-board temperature (left y-axis) and peak power (right y-axis) over a 7-minute illumination (measurements taken at 1-second interval). Peak power was measured along the optical axis at the well-plate surface.

The light field at the plate surface was analyzed for uniformity by acquiring measurements centered at the positions of each of the 4 wells being treated simultaneously (Fig. **5**). It was determined that the variations in the power delivered to each well were 2.3% for both arrays. At operating temperature (39°C), the intensity was 86.6 ± 2.0 mW/cm^2 (CV = 2.3%) for the 635 nm array and 79.7 ± 1.8 mW/cm^2 (CV = 2.3%) for the 690 nm array. Individual well measurements were further analyzed to check for inhomogeneities in the light field. It was determined that for the 635 nm module, the power delivered to well A2 was 3.9 mW/cm^2 (4.3%) larger than to A1 (p = 0.0207) and B2 (p = 0.0207) but was no different from B1 (p = 0.2594), indicating a minute non-uniformity in the photon flux through the aperture. No differences in light delivery from 690 nm module were detected (p = 0.3081).

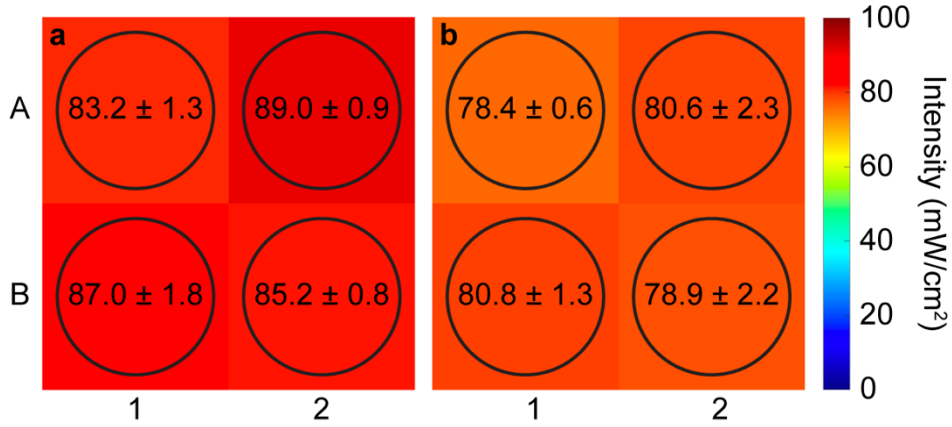

Fig. 5 Light field assessment of the (**a**) 635 nm and (**b**) 690 nm LED modules. Intensity was measured in each quadrant of the 3.85×3.85-cm aperture to estimate the power delivered to each well of a 2×2-well experimental group (A1–B2). Circles represent approximate location and area of the power meter sensor within each quadrant of the aperture. Results are mean ± SD of 3 measurements. One-way ANOVA of the 4 quadrant measurements was significant for the 635 nm array (p = 0.0142) and not significant for the 690 nm array (p = 0.3081). Follow-up analysis with Tukey's multiple comparisons test on the 635 nm array group revealed the intensity in well A2 was significantly larger than A1 (p = 0.0207) and B2 (p = 0.0207), but not different from B1 (p = 0.2594). Reported p-values are adjusted for multiple comparisons.

3.3 PDT

A primary ovarian cancer cell line was successfully treated with ALA- and BPD-PDT using the 635 nm and 690 nm modular LED arrays, respectively. A clear, light-dependent decrease in cell viability was

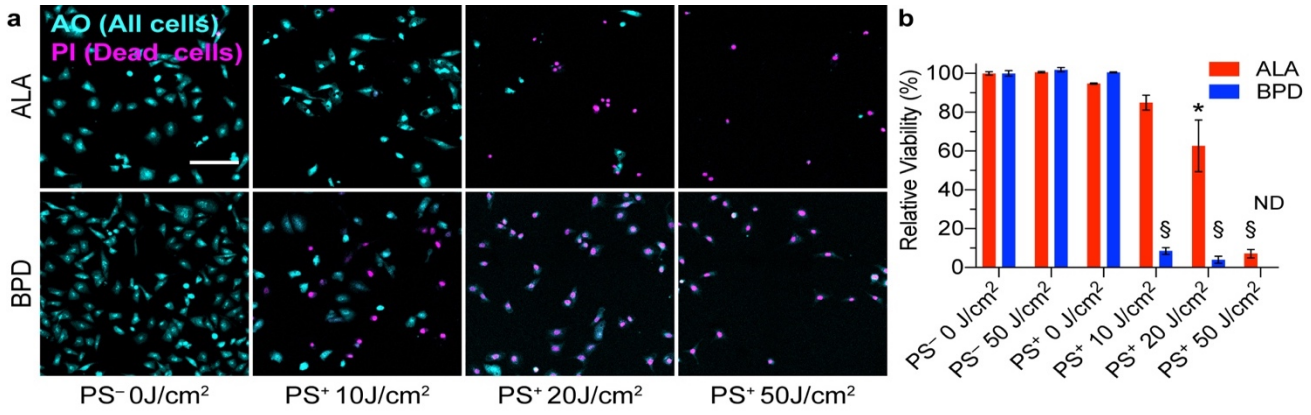

Fig. 6. Viability of Powder cells 24 hours post LED-PDT. (**a**) Acridine orange (AO) / Propidium Iodide (PI) staining shows PDT induced cell death. Full images are provided in Fig. **S5**. Scale bar, 200 µm. (**b**) Viability assesed by Live/Dead flow cytometry staining (n = 3 biological replicates) confirms a light dose-dependant response to treatment. One-way ANOVA for each experiment was significant ($p < 0.0001$), and Dunnett's multiple comparisons test confirmed siginficant differences comnpared to the control group. $^{*}p = 0.0025$, $^{\S}p < 0.0001$, ND = Not Detected. p-values are adjusted for multiple comparisons.

observed via fluorescence microscopy and quantified with Live/Dead FC analysis (Fig. **6**). Compared to the no-light, no-PS control, cell viability was 63 ± 13% (p = 0.0025) after 20 J/cm^2 and 7 ± 2% ($p <$ 0.0001) after 50 J/cm^2 of ALA-PDT. Similarly, only 9 ± 2% ($p < 0.0001$) and 4 ± 2% ($p < 0.0001$) of cells remained viable after 10 and 20 J/cm^2 of BPD-PDT, respectively. No cells were detected by FC 24 hours after the 50 J/cm^2 dose of BPD-PDT, so viability was unable to be quantified. However, imaging confirms near complete cell death consistent with the dose-response trend. Full images are provided in Fig. **S5**.

4 Discussion

This work describes a benchtop PDT device to facilitate economical multi-PS photodynamic therapy research. The device incorporates a modular design built around high-power surface mounted LEDs. Due to the significant heat generated by such LEDs, an aluminum PCB, heat sink, and active air cooling were incorporated to maximize heat flow away from the LEDs. With active cooling, the module temperature (and therefore power) can be operated at stable equilibrium with < 1% fluctuation over the course of PDT. The system was successfully used to treat a monolayer ovarian cancer model with both ALA and verteporfin wherein both experiments were performed on the same day, thus confirming its multi-PS versatility and practicality.

Beyond the present configuration, the device allows for flexibility in experimental design in many aspects. First, the modular design allows experimenters to add additional wavelengths quickly and at very low cost (~$150 per module, plus, excluding the computer, power meter, and 3D printer, ~$2000 of supporting materials as a one-time investment). This provides a significant advantage to investigators developing and testing new PSs for which commercial light sources would be prohibitively costly (*e.g.*, a laser) or do not exist. The simple swapping of modules allows activation of different PSs within minutes, opening the door for development of combination PDT[42–44] (as has been done extensively with chemotherapy). Additionally, the digital shutter allows for implementation of complex fractionated[45–47] and metronomic[48] phototherapeutic strategies.

Second, the large spot size (~4×4 cm) provides for flexible use of different well plates for various applications. Here, we designed a fixed aperture to illuminate a 2×2-well group in a 24-well plate for simultaneous treatment of 4 biological replicates. In principle, other microplate sizes or dishes could be illuminated with varying sizes and groupings, or the aperture could be constricted to single-well illumination. Although a reduced spot size would provide a larger average power across the well, this would also increase the number of trials per plate and therefore the total plate illumination time. This is the main limitation of laser-based systems we set out to overcome. Experimenters should take care to keep total plate treatment times short to avoid significant auxiliary cell death. This flexibility in well-plate design is programmed into the ExpressPDT software to allow for a custom grid of desired light doses per plate.

Finally, extension of this protocol to *in vivo* work is also feasible, as the plexiglass surface is suitable to support small animal models. For example, subcutaneous tumors in a mouse model could be epi-illuminated using the described configuration. In this work we show that a clinically relevant 50 J/cm^2 dose is practical and was enough to achieve >90% cell death in monolayer cell culture with multiple PSs.

For large tumors, doses as high as 200 J/cm^2 are attainable (~32 minutes per dose at peak power). Of course, tissue oxygen becomes an important factor for *in vivo* PDT[45], and doses larger than 40–50 J/cm^2 present with diminishing therapeutic returns[10]. As mentioned above, an automated fractionation protocol becomes an important component of high-dose PDT, which may be developed and tested both *in vitro* and *in vivo* using this device.

Further optimizations would improve the device for future implementations. First, including a photodiode would allow for automated power monitoring after calibration similar to the method for thermistor calibration described herein. Second, denser arrays with a larger footprint could be designed to provide a more uniform spot size for larger treatment groups or even whole-plate illumination. Third, off-the-shelf water-cooling systems for high-power computer CPUs could also be adopted to provide a more efficient cooling system for the board, allowing the LEDs to operate at higher powers and reducing the risk of thermal damage to the board or its components. However, water cooling may be undesirable for a mobile-cart implementation. Finally, an investigation into the lifespan of the LED module was not done here but may be warranted for instances of high-throughput use.

In summary, we devised a versatile and cost-effective device to enable and improve the forefront of PDT research. Design of the LED module for efficient heat transfer enabled stable high-power output, which was used as an effective treatment of a primary ovarian cancer model *in vitro*. The modular design begets a low cost-per-wavelength device to facilitate next-generation, multi-PS research, which is not practical with existing commercial light sources. Additionally, a custom application, ExpressPDT, is included for streamlined experimental planning and semi-automated protocol implementation. This work is intended to aid the research community in developing the next generation of phototherapy and photodynamic therapy using LEDs as valuable and versatile light source.

5 Acknowledgements

We thank Dr. Jason Sutin for advising construction of the aluminum PCB and the Institute for Chemical Imaging of Living Systems at Northeastern University for assistance with image acquisition. This work was supported by the Northeastern University Alpha Fund Program (to E.M.K), National Institutes of Health Grant K22CA181611 (to B.Q.S.) and the Richard and Susan Smith Family Foundation (Newton, MA) Smith Family Award for Excellence in Biomedical Research (to B.Q.S.).

6 Disclosures

The authors declare no conflicts of interests.

7 References

1. A. Grzybowski, J. Sak, and J. Pawlikowski, "A brief report on the history of phototherapy," Clin Dermatol **34**(5), 532–537 (2016) [doi:10.1016/j.clindermatol.2016.05.002].

2. H. Hönigsmann, "History of phototherapy in dermatology," Photochem Photobio S **12**(1), 16–21 (2012) [doi:10.1039/c2pp25120e].

3. M. A. Pathak and T. B. Fitzpatrick, "The evolution of photochemotherapy with psoralens and UVA (PUVA): 2000 BC to 1992 AD," J Photochem Photobiology B Biology **14**(1–2), 3–22 (1992) [doi:10.1016/1011-1344(92)85080-e].

4. U. Khanna and S. Khandpur, "What is new in narrow-band ultraviolet-B therapy for vitiligo?," Indian Dermatology Online J **10**(3), 234 (2019) [doi:10.4103/idoj.idoj_310_18].

5. J. Foerster et al., "Narrowband UVB treatment is highly effective and causes a strong reduction in the use of steroid and other creams in psoriasis patients in clinical practice," Plos One **12**(8), e0181813 (2017) [doi:10.1371/journal.pone.0181813].

6. J. Chen et al., "New Technology for Deep Light Distribution in Tissue for Phototherapy," Cancer J **8**(2), 154–163 (2002) [doi:10.1097/00130404-200203000-00009].

7. T. Dougherty et al., "Photoradiation therapy for the treatment of malignant tumors.," Cancer Res **38**(8), 2628–2635 (1978).

8. A. D. White, "Recollections of the First Continuous Visible Laser," Opt Photonics News **22**(10), 34 (2011) [doi:10.1364/opn.22.10.000034].

9. D. Kessel, “More Adventures in Photodynamic Therapy,” Int J Mol Sci **16**(7), 15188–15193 (2015) [doi:10.3390/ijms160715188].

10. L. Brancaleon and H. Moseley, “Laser and Non-laser Light Sources for Photodynamic Therapy,” Laser Med Sci **17**(3), 173–186 (2002) [doi:10.1007/s101030200027].

11. B. C. Wilson and M. S. Patterson, “The physics, biophysics and technology of photodynamic therapy,” Phys Med Biol **53**(9), R61 (2008) [doi:10.1088/0031-9155/53/9/r01].

12. M. R. Avram, M. M. Avram, and P. M. Friedman, “Laser and Light Source Treatments for the Skin” (2014).

13. D. Oda et al., “Antimicrobial action of photodynamic therapy in root canals using LED curing light, curcumin and carbopol gel,” Int Endod J **52**(7), 1010–1019 (2019) [doi:10.1111/iej.13092].

14. T. J. Dougherty et al., “Photodynamic Therapy,” Jnci J National Cancer Inst **90**(12), 889–905 (1998) [doi:10.1093/jnci/90.12.889].

15. J. Moan and Q. Peng, “An outline of the hundred-year history of PDT.,” Anticancer Res **23**(5A), 3591–3600 (2003).

16. J. Moan and Q. Peng, “An outline of the history of PDT,” 1–18 (2003) [doi:10.1039/9781847551658-00001].

17. P. Agostinis et al., “Photodynamic therapy of cancer: An update,” Ca Cancer J Clin **61**(4), 250–281 (2011) [doi:10.3322/caac.20114].

18. K. Plaetzer et al., “Photophysics and photochemistry of photodynamic therapy: fundamental aspects,” Laser Med Sci **24**(2), 259–268 (2009) [doi:10.1007/s10103-008-0539-1].

19. J. Zhang et al., “An updated overview on the development of new photosensitizers for anticancer photodynamic therapy,” Acta Pharm Sinica B **8**(2), 137–146 (2018) [doi:10.1016/j.apsb.2017.09.003].

20. R. R. Allison and C. H. Sibata, “Oncologic photodynamic therapy photosensitizers: A clinical review,” Photodiagn Photodyn **7**(2), 61–75 (2010) [doi:10.1016/j.pdpdt.2010.02.001].

21. “Levulan Kerastick FDA Label” (2018).

22. A. Juzeniene et al., “Effectiveness of different light sources for 5-aminolevulinic acid photodynamic therapy,” Laser Med Sci **19**(3), 139–149 (2004) [doi:10.1007/s10103-004-0314-x].

23. P. Babilas et al., “Split-face-study using two different light sources for topical PDT of actinic keratoses:non-inferiority of the LED system,” Jddg J Der Deutschen Dermatologischen Gesellschaft **6**(1), 25–32 (2008) [doi:10.1111/j.1610-0387.2007.06555.x].

24. R.-M. Szeimies et al., “Photodynamic therapy for non-melanoma skin cancer.,” Acta Derm-venereol **85**(6), 483–490 (2005).

25. D. T. Tran and R. Salmon, “Field treatment of facial and scalp actinic keratoses with photodynamic therapy: Survey of patient perceptions of treatment satisfaction and outcomes,” Australas J Dermatol **52**(3), 195–201 (2011) [doi:10.1111/j.1440-0960.2011.00785.x].

26. “Visudyne (Verteporfin for Injection) FDA Label” (2012).

27. M. de Chaves et al., “Effects of low-power light therapy on wound healing: LASER x LED,” An Bras Dermatol **89**(4), 616–623 (2014) [doi:10.1590/abd1806-4841.20142519].

28. M. E. Etcheverry, M. A. Pasquale, and M. Garavaglia, “Photodynamic therapy of HeLa cell cultures by using LED or laser sources,” J Photochem Photobiology B Biology **160**, 271–277 (2016) [doi:10.1016/j.jphotobiol.2016.04.013].

29. H. Takahashi et al., “Photodynamic therapy using a novel irradiation source, LED lamp, is similarly effective to photodynamic therapy using diode laser or metal-halide lamp on DMBA- and TPA-induced mouse skin papillomas,” J Dermatology **41**(8), 729–731 (2014) [doi:10.1111/1346-8138.12572].

30. S. Mallidi et al., “In vivo evaluation of battery-operated light-emitting diode-based photodynamic therapy efficacy using tumor volume and biomarker expression as endpoints,” J Biomed Opt **20**(4), 048003–048003 (2015) [doi:10.1117/1.jbo.20.4.048003].

31. N. Neittaanmäki-Perttu et al., “Photodynamic Therapy for Actinic Keratoses: A Randomized Prospective Non-sponsored Cost-effectiveness Study of Daylight-mediated Treatment Compared with Light-emitting Diode Treatment.,” Acta Derm-venereol **96**(2), 241–244 (2016) [doi:10.2340/00015555-2205].

32. E. Sorbellini, M. Rucco, and F. Rinaldi, “Photodynamic and photobiological effects of light-emitting diode (LED) therapy in dermatological disease: an update,” Laser Med Sci **33**(7), 1431–1439 (2018) [doi:10.1007/s10103-018-2584-8].

33. H. Moseley, “Light distribution and calibration of commercial PDT LED arrays,” Photochem Photobiol Sci **4**(11), 911–914 (2005) [doi:10.1039/b507325a].

34. A. Borba et al., “Photodynamic therapy with high-power LED mediated by erythrosine eliminates Enterococcus faecalis in planktonic forms,” Photodiagn Photodyn **19**, 348–351 (2017) [doi:10.1016/j.pdpdt.2017.07.007].

35. C. D. Enk and A. Levi, “Low-irradiance red LED traffic lamps as light source in PDT for actinic keratoses,” Photodermatol Photoimmunol Photomed **28**(6), 332–334 (2012) [doi:10.1111/j.1600-0781.2012.00694.x].

36. G. Kim and A. Gaitas, “Extracorporeal Photo-Immunotherapy for Circulating Tumor Cells,” Plos One **10**(5), e0127219 (2015) [doi:10.1371/journal.pone.0127219].

37. Z. Jamali et al., “Effects of LED-Based photodynamic therapy using red and blue lights, with natural hydrophobic photosensitizers on human glioma cell line,” Photodiagn Photodyn **21**, 50–54 (2018) [doi:10.1016/j.pdpdt.2017.11.002].

38. L. Duse et al., “Low level LED photodynamic therapy using curcumin loaded tetraether liposomes,” Eur J Pharm Biopharm **126**(Bioorg. Med. Chem. 13 2005), 233–241 (2017) [doi:10.1016/j.ejpb.2017.10.005].

39. D. Chen et al., “Light-Emitting Diode-Based Illumination System for In Vitro Photodynamic Therapy,” Int J Photoenergy **2012**, 1–6 (2012) [doi:10.1155/2012/920671].

40. J. Hempstead et al., “Low-cost photodynamic therapy devices for global health settings: Characterization of battery-powered LED performance and smartphone imaging in 3D tumor models,” Sci Rep-uk **5**(1), 10093 (2015) [doi:10.1038/srep10093].

41. T. Araújo et al., “Reduced methicillin-resistant Staphylococcus aureus biofilm formation in bone cavities by photodynamic therapy,” Photodiagn Photodyn **21**(BMC Microbiol. 9 1 2009), 219–223 (2018) [doi:10.1016/j.pdpdt.2017.12.011].

42. L. Cincotta et al., “Benzophenothiazine and Benzoporphyrin Derivative Combination Phototherapy Effectively Eradicates Large Murine Sarcomas,” Photochem Photobiol **63**(2), 229–237 (1996) [doi:10.1111/j.1751-1097.1996.tb03019.x].

43. A. Villanueva et al., “A new protocol in photodynamic therapy: enhanced tumour cell death by combining two different photosensitizers,” Photochem Photobiol Sci **9**(3), 295–297 (2010) [doi:10.1039/b9pp00153k].

44. D. Kessel and J. J. Reiners, “Enhanced Efficacy of Photodynamic Therapy via a Sequential Targeting Protocol,” Photochem Photobiol **90**(4), 889–895 (2014) [doi:10.1111/php.12270].

45. T. H. Foster et al., “Oxygen Consumption and Diffusion Effects in Photodynamic Therapy,” Radiat Res **126**(3), 296 (1991) [doi:10.2307/3577919].

46. S. Müller et al., “Enhanced photodynamic effects using fractionated laser light,” J Photochem Photobiology B Biology **42**(1), 67–70 (1998) [doi:10.1016/s1011-1344(97)00124-3].

47. A. de Souza et al., “Comparing desferrioxamine and light fractionation enhancement of ALA-PpIX photodynamic therapy in skin cancer,” Brit J Cancer **115**(7), 805 (2016) [doi:10.1038/bjc.2016.267].

48. S. K. Bisland et al., “Metronomic Photodynamic Therapy as a New Paradigm for Photodynamic Therapy: Rationale and Preclinical Evaluation of Technical Feasibility for Treating Malignant Brain Tumors,” Photochem Photobiol **80**(1), 22–30 (2004) [doi:10.1111/j.1751-1097.2004.tb00044.x].